

An eddy-viscosity subgrid-scale model for turbulent shear flow: Algebraic theory and applications

A. W. Vreman^{a)}

Vreman Research, Godfried Bomansstraat 46, 7552 NT Hengelo, The Netherlands

(Received 16 April 2004; accepted 24 June 2004; published online 1 September 2004)

An eddy-viscosity model is proposed and applied in large-eddy simulation of turbulent shear flows with quite satisfactory results. The model is essentially not more complicated than the Smagorinsky model, but is constructed in such a way that its dissipation is relatively small in transitional and near-wall regions. The model is expressed in first-order derivatives, does not involve explicit filtering, averaging, or clipping procedures, and is rotationally invariant for isotropic filter widths. Because of these highly desirable properties the model seems to be well suited for engineering applications. In order to provide a foundation of the model, an algebraic framework for general three-dimensional flows is introduced. Within this framework several types of flows are proven to have zero energy transfer to subgrid scales. The eddy viscosity is zero in the same cases; the theoretical subgrid dissipation and the eddy viscosity have the same algebraic structure. In addition, the model is based on a fundamental realizability inequality for the theoretical subgrid dissipation. Results are shown for a transitional and turbulent mixing layer at high Reynolds number and a turbulent channel flow. In both cases the present model is found to be more accurate than the Smagorinsky model and as good as the standard dynamic model. Unlike the Smagorinsky model, the present model is able to adequately handle not only turbulent but also transitional flow. © 2004 American Institute of Physics. [DOI: 10.1063/1.1785131]

I. INTRODUCTION

The development of subgrid models for large-eddy simulation (LES) is an important area in turbulence research (see the reviews in Refs. 1 and 2). Eddy-viscosity models are popular, since they are robust in practice and principally respect the dissipative character of turbulence. An accurate eddy viscosity for inhomogeneous turbulent flow should become small in laminar and transitional regions. This requirement is unfortunately not satisfied by existing simple eddy-viscosity closures such as the well-known Smagorinsky model.³ Germano *et al.*⁴ solved this problem by the application of a dynamic procedure to the Smagorinsky model. The common implementation of the dynamic procedure incorporates explicit filtering operations, ensemble averaging in homogeneous directions, and a somewhat *ad hoc* clipping to prevent an unstable (negative) eddy viscosity. The extension of these techniques to complex flows is not trivial, which is an important reason to continue the search for an eddy viscosity that performs reasonably well without additional procedures.

LES with an eddy-viscosity closure solves the filtered Navier–Stokes equations,

$$\partial_j \bar{u}_j = 0, \quad (1)$$

$$\partial_i \bar{u}_i + \partial_j (\bar{u}_i \bar{u}_j) = -\partial_i (\bar{p} + \tau_{kk}/3) + \nu \partial_j^2 \bar{u}_i + \partial_j (2\nu_e S_{ij}), \quad (2)$$

using the summation convention for repeated indices. The unknown turbulent stress tensor

$$\tau_{ij} = \overline{u_i u_j} - \bar{u}_i \bar{u}_j \quad (3)$$

has been replaced by the model

$$-2\nu_e S_{ij} + \tau_{kk} \delta_{ij}/3, \quad (4)$$

where $S_{ij} = \frac{1}{2} \partial_i \bar{u}_j + \frac{1}{2} \partial_j \bar{u}_i$.

The following eddy viscosity is proposed in the present paper:

$$\nu_e = c \sqrt{\frac{B_\beta}{\alpha_{ij} \alpha_{ij}}}, \quad (5)$$

with

$$\alpha_{ij} = \partial_i \bar{u}_j = \frac{\partial \bar{u}_j}{\partial x_i}, \quad (6)$$

$$\beta_{ij} = \Delta_m^2 \alpha_{mi} \alpha_{mj}, \quad (7)$$

$$B_\beta = \beta_{11} \beta_{22} - \beta_{12}^2 + \beta_{11} \beta_{33} - \beta_{13}^2 + \beta_{22} \beta_{33} - \beta_{23}^2. \quad (8)$$

The model constant c is related to the Smagorinsky constant C_S by $c \approx 2.5C_S^2$. Like the Smagorinsky model, this model is easy to compute in actual LES, since it does not need more than the local filter width and the first-order derivatives of the velocity field.

The symbol α represents the (3×3) matrix of derivatives of the filtered velocity \bar{u} . If $\alpha_{ij} \alpha_{ij}$ equals zero, ν_e is consistently defined as zero. The tensor β is proportional to the gradient model^{5,6} in its general anisotropic form.⁷ It is positive semidefinite,⁸ which implies $B_\beta \geq 0$. In fact, B_β is an invariant of the matrix β , while $\alpha_{ij} \alpha_{ij}$ is an invariant (trace)

^{a)}Electronic mail: bert@vremanresearch.nl

of $\alpha^T \alpha$. Therefore, model (5) is invariant under a rotation of the coordinate axes, in case the filter width is the same in each direction ($\Delta_i = \Delta$ implies $\beta = \Delta^2 \alpha^T \alpha$).

In Sec. II a theoretical foundation of model (5) will be provided using algebraic inequalities and classifications, which will demonstrate that the model and the theoretical subgrid dissipation vanish for the same types of flow. In Sec. III the model will be applied to LES of a mixing layer and a channel flow.

II. THEORY

In this section it will be shown how model (5) emerges from the investigation of algebraic properties of the theoretical subgrid dissipation. We will distinguish between 320 types of flows and algebraically classify these flows into ten groups. The theoretical subgrid dissipation will be proven to be zero for 13 laminar flow types. Next we will consider flow functionals which are entirely expressed in first-order velocity derivatives. In particular the functional B_β , used in the model (5), exactly vanishes for the 13 laminar flow types mentioned above. An upper bound proportional for the theoretical subgrid dissipation will also be derived and this realizability condition will indicate how B_β should be used in actual models. Other inequalities will be employed to estimate the value of the model coefficient c .

The theoretical subgrid dissipation is usually defined by

$$D_\tau = -\tau_{ij} \alpha_{ij} = -\tau_{ij} S_{ij}, \tag{9}$$

which can be rewritten as

$$D_\tau = -(\tau, \alpha) = -(\tau, S), \tag{10}$$

where (\cdot, \cdot) is an inner product for the space of (3×3) matrices, similar to \mathbb{R}^9 . The inner product defines the norm $\|\tau\|^2 = (\tau, \tau)$. In this way zero subgrid dissipation means that τ is orthogonal to α and S .

In practice it is often desirable to adopt a nonuniform filter, in order to allow a spatially variable filter width. It is well known that for nonuniform filters the commutation between spatial derivatives and the filter is lost. Consequently, the dissipation from resolved to subgrid scales is not governed by D_τ only, but is also influenced by the so-called commutator errors. The commutator errors make a rigorous mathematical treatment of the nonuniformly filtered equations much more difficult, although it can be proven that global conservation of mass and momentum is ensured for self-adjoint nonuniform filters.⁹ In this paper we assume commutation between filter and spatial derivative. Thus we presently neglect the dissipation caused by the commutator errors and optimize the algebraic structure of the eddy viscosity by considering D_τ only. In the practical implementation of the model the filter does not explicitly occur, only the filter width, which can easily be taken nonuniform. This does not mean that the subgrid model and the implicit (basic) filter are independent, since the model replaces the exact turbulent stress, whose distribution and magnitude depend strongly on the order property and cutoff of the basic filter.¹⁰ In this section we will first derive that for arbitrary commutative filters the property $D_\tau = 0$ is satisfied in the case of at least 13

flow classes. Afterwards, the spherical top-hat filter will play an important role to prove that $D_\tau = 0$ does not hold in general for other entire flow classes (see the Appendix).

In the following we thus derive that D_τ vanishes for certain types of derivative matrices of unfiltered velocities, $\chi_{ij} = \partial_i u_j$. Consider a fixed location x in Ω and an open local space Ω_x around x . Let Γ be the space of all three-dimensional kernel filters G which (1) are linear and normalized, (2) have a closed support Ω'_x inside Ω_x , and (3) commute with spatial derivatives. A robust eddy viscosity should not unnecessarily become zero, so we try to find the flows that have zero subgrid dissipation without imposing more restrictions on the filter.

Using the linearity and normalization of the filter, the turbulent stress tensor can be written as⁸

$$\begin{aligned} \tau_{ij} &= \overline{u_i u_j}(x) - \bar{u}_i(x) \bar{u}_j(x) - \bar{u}_j(x) \bar{u}_i(x) + \bar{u}_i(x) \bar{u}_j(x) \\ &= \int_{\Omega'_x} G(x, y) [u_i(y) - \bar{u}_i(x)] [u_j(y) - \bar{u}_j(x)] dy = \overline{v_i^x v_j^x}, \end{aligned} \tag{11}$$

where $v_i^x(y) = u_i(y) - \bar{u}_i(x)$, which is unequal to the usual u_i' . This reformulation immediately shows that $\tau_{ij} = 0$ if u_i or u_j is constant on Ω_x . It is remarked that constant u_i on Ω_x implies zero $\partial_m u_i$ on Ω_x and zero $\partial_m \bar{u}_i$ in x .

To find local flow types with $D_\tau = 0$ in x , we start with one constant velocity component, say u_1 . Consequently, τ_{1j} , $\partial_i u_1$, and $\partial_i \bar{u}_1$ are zero. Then the condition $(\tau, \alpha) = 0$ reduces to

$$\tau_{22} \partial_2 \bar{u}_2 + \tau_{23} \partial_2 \bar{u}_3 + \tau_{23} \partial_3 \bar{u}_2 + \tau_{33} \partial_3 \bar{u}_3 = 0. \tag{12}$$

This equation is satisfied if, for example,

$$\partial_2 \bar{u}_2 = \partial_2 \bar{u}_3 = \partial_3 \bar{u}_2 = \partial_3 \bar{u}_3 = 0. \tag{13}$$

Only two derivatives are allowed to be nonzero; the theoretical subgrid dissipation is zero if

$$\chi_{ij} = \begin{pmatrix} 0 & \partial_1 u_2 & \partial_1 u_3 \\ 0 & 0 & 0 \\ 0 & 0 & 0 \end{pmatrix} \tag{14}$$

on Ω_x .

The only other possibilities to satisfy Eq. (12) for an entire class require zero τ_{22} , τ_{23} , or τ_{33} . To achieve this, an additional constant velocity component is necessary, say u_2 , which implies zero τ_{2j} . Finally $\partial_3 u_3$ and consequently $\partial_3 \bar{u}_3$ have to be zero, and then Eq. (12) is satisfied. The derivative matrix that is left over leads to a zero subgrid dissipation:

$$\chi_{ij} = \begin{pmatrix} 0 & 0 & \partial_1 u_3 \\ 0 & 0 & \partial_2 u_3 \\ 0 & 0 & 0 \end{pmatrix} \tag{15}$$

on Ω_x . The matrices (14) and (15) represent simple locally laminar shear flows.

The arguments can be repeated with a cyclic interchange of indices: $1 \rightarrow 2 \rightarrow 3 \rightarrow 1$. The total result consists of six matrices with the following pairs of nonzero components: $\{\partial_1 u_2, \partial_1 u_3\}$; $\{\partial_2 u_1, \partial_2 u_3\}$; $\{\partial_3 u_1, \partial_3 u_2\}$ and $\{\partial_2 u_1, \partial_3 u_1\}$;

TABLE I. The number of elements in $Q_n(J)$, that is, the number of flow types with n zero derivatives and $J=0$. A blank space means zero elements.

| J | Q_{0-2} | Q_3 | Q_4 | Q_5 | Q_6 | Q_7 | Q_8 | Q_9 | Q_{0-9} |
|-----------|-----------|-------|-------|-------|-------|-------|-------|-------|-----------|
| 0 | 43 | 66 | 81 | 66 | 39 | 18 | 6 | 1 | 320 |
| D_τ | | | | | | 6 | 6 | 1 | 13 |
| $\ S\ $ | | | | | | | | 1 | 1 |
| A_β | | | | | | | | 1 | 1 |
| B_β | | | | | | 6 | 6 | 1 | 13 |
| C_β | | 6 | 30 | 48 | 36 | 18 | 6 | 1 | 145 |
| D_β | | | | 3 | 14 | 15 | 6 | 1 | 39 |

$\{\partial_1 u_2, \partial_3 u_2\}; \{\partial_1 u_3, \partial_2 u_3\}$. This includes the trivial solution with nine zero velocity derivatives and the six possibilities of the simplest shear flows, which have only one nonzero velocity derivative $\partial_i u_j$ with $i \neq j$. The Appendix proves that the types of derivative matrices with $D_\tau=0$ are restricted to the ones just mentioned, in case no additional limitations are imposed on the filter.

To formalize the approach above, an algebraic classification will be introduced that distinguishes between 320 types of flows, separated into ten classes. For a given number n and flow functional J we define the set of flow types for which the derivative matrix has n zeros and $J=0$. The corresponding sets of binary matrices are called the ‘‘flow algebra’’ of J .

For this purpose we define an operator that transforms a matrix field into a binary matrix:

$$(P\chi)_{ij} = \begin{cases} 0 & \text{if } \chi_{ij} = 0 \text{ on } \Omega_x \\ 1 & \text{if } \chi_{ij} \neq 0 \text{ on } \Omega_x. \end{cases} \quad (16)$$

A velocity field is not divergence-free if its derivative matrix χ has precisely one nonzero diagonal element. Therefore, we define Z as the set of all binary matrices except those that have precisely one nonzero diagonal elements. The set Z contains $2^9 - 3 \times 2^6 = 320$ matrices. In addition the class Z_n denotes the set of all binary matrices in Z with n zero elements. The case $J=0$ in Table I lists the number of elements within each class.

For a given flow functional J , for example, the subgrid dissipation, we define

$$Q_n(J) = \{\zeta \in Z_n \mid (\forall u)(\forall G \in \Gamma)(P\chi = \zeta \Rightarrow J=0)\}, \quad (17)$$

where χ is the unfiltered velocity derivative matrix. The set $Q_n(J)$ represents all local flow types with n zero velocity derivatives and $J=0$. We call the collection $\{Q_n(J)\}$ the *flow algebra* of J .

The flow algebra for the theoretical subgrid dissipation D_τ has been derived above and the sizes of $Q_n(D_\tau)$ are summarized in the second line of Table I. Table I also summarizes the flow algebras of five functionals that are entirely based on the filtered velocity derivative matrix. An algebraic computer program was developed to obtain these results. The most important and relatively small flow algebra is listed in the Appendix. This flow algebra consists of 13 matrices. There are only two fundamentally different solutions, repre-

sented by Eqs. (14) and (15). The other eleven matrices can be derived from these two types by cyclic interchange of indices and/or setting one or two nonzero elements to zero.

A certain functional J might be a good candidate to incorporate into an eddy viscosity if $\{Q_n(J)\}$ is close to $\{Q_n(D_\tau)\}$. The first functional investigated is $\|S\|^2$, relevant for the Smagorinsky eddy viscosity $C_S^2 \Delta^2 |S|$ with $|S|^2 = 2\|S\|^2$. The other functionals are based on β , defined by Eq. (7):

$$A_\beta = 2k_\beta = \beta_{ii} = \lambda_1 + \lambda_2 + \lambda_3, \quad (18)$$

$$B_\beta = \beta_{11}\beta_{22} - \beta_{12}^2 + \beta_{11}\beta_{33} - \beta_{13}^2 + \beta_{22}\beta_{33} - \beta_{23}^2 \\ = \lambda_1\lambda_2 + \lambda_1\lambda_3 + \lambda_2\lambda_3, \quad (19)$$

$$C_\beta = \det \beta = \lambda_1\lambda_2\lambda_3, \quad (20)$$

$$D_\beta = -(\beta, S) = -\beta_{ij}S_{ij}. \quad (21)$$

The eigenvalues λ_i are the roots of the characteristic polynomial. Like the eigenvalues, the coefficients of the polynomial, A_β , B_β , and C_β , are invariant under rotation. As β is positive semidefinite, each λ_i is a positive real number. Consequently, A_β , B_β , and C_β are always positive, unlike the dissipation of the gradient model D_β .

In one case the flow algebra is exactly the same as for the theoretical subgrid dissipation; the sets $\{Q_n(B_\beta)\}$ and $\{Q_n(D_\tau)\}$ are identical (see the Appendix), which means that B_β and D_τ vanish for the same types of flow. Thus, for inhomogeneous turbulence the algebraic theory strongly supports an eddy viscosity based on B_β . The fact that B_β is positive allows us to define positive eddy viscosities in a natural way; *ad hoc* procedures to avoid negative diffusion are not required.

The Smagorinsky eddy viscosity, proportional to $\|S\|$, only vanishes in the trivial case $\chi=0$, like A_β . Compared to D_τ , the flow algebras of C_β and D_β are too large. The matrices

$$\begin{pmatrix} 0 & \partial_1 u_2 & 0 \\ 0 & 0 & \partial_2 u_3 \\ \partial_3 u_1 & 0 & 0 \end{pmatrix}, \quad \begin{pmatrix} 0 & \partial_1 u_2 & 0 \\ \partial_2 u_1 & 0 & \partial_2 u_3 \\ 0 & \partial_3 u_2 & 0 \end{pmatrix} \quad (22)$$

are examples for which D_β is zero. Due to the relatively large size of the flow algebra, the dissipation of models based on C_β and D_β might be insufficient. In addition, D_β is not always positive. Consequently, simulations¹¹ which use an eddy-viscosity proportional to D_β suffer from numerical instabilities, unless additional techniques are applied, such as clipping or ensemble averaging in the dynamic model. The positiveness of B_β is clearly an advantage.

To propose an appropriate relationship between ν_e and B_β , a realizability argument for ν_e is used. For positive filters, τ is positive semidefinite,⁸ which implies

$$\|\tau\| \leq A_\tau = 2k_\tau, \quad (23)$$

$$0 \leq 3B_\tau \leq A_\tau^2 = 4k_\tau^2, \quad (24)$$

$$0 \leq 27C_\tau \leq A_\tau^3. \tag{25}$$

The first inequality is proven with use of the realizability conditions for τ , for example, $\tau_{12}^2 \leq \tau_{11}\tau_{22}$. The other inequalities can be proven by maximizing the functions B_τ/A_τ and C_τ/A_τ after the substitution of $r=\lambda_2/\lambda_1 \leq 1$ and $s=\lambda_3/\lambda_1 \leq 1$ into Eqs. (18) and (20).

A fundamental result for the theoretical subgrid dissipation is obtained if the Schwarz inequality and inequality (23) are applied:

$$D_\tau = -(\tau, S) \leq \|\tau\| \|S\| \leq 2k_\tau \|S\|. \tag{26}$$

This means that the theoretical subgrid dissipation is bounded by a term which is proportional to the subgrid kinetic energy. If the filter is replaced by the Reynolds averaging operator, the inequality expresses an upper bound for the standard turbulent production.

The modeled subgrid dissipation, $2\nu_e \|S\|^2$, ideally equals D_τ . In that case, inequality (26) results in the following realizability condition:

$$\nu_e \leq k_\tau \|S\|^{-1}. \tag{27}$$

Compare Ref. 8, where a similar inequality was derived to estimate k for eddy-viscosity models.

Condition (27) is satisfied by the following class of eddy viscosities:

$$\nu_e = \frac{c_0 k_\tau^{1-2q} (\frac{3}{4} B_\tau)^q}{\|\alpha\|} \leq \frac{c_0 k_\tau}{\|\alpha\|} \leq \frac{c_0 k_\tau}{\|S\|} \tag{28}$$

with $q \geq 0$ and $c_0 \leq 1$, while we used

$$\|S\| = \frac{1}{2} \|\alpha + \alpha^T\| \leq \frac{1}{2} \|\alpha\| + \frac{1}{2} \|\alpha^T\| = \|\alpha\|. \tag{29}$$

It is remarked that for one-equation models¹² with $\nu_e = c_k \Delta \sqrt{k_r}$, condition (27) implies $\nu_e \geq c_k^2 \Delta^2 \|S\|$, expressing that ν_e should always be larger than some Smagorinsky model. From the perspective of realizability, it would be more logical to define $\nu_e = c_k k_r \|\alpha\|^{-1}$, that is, Eq. (28) for $q = 0$.

A family of practical models is obtained from definition (28) if k_τ and B_τ are replaced by k_β and B_β :

$$\nu_e = \frac{c k_\beta^{1-2q} B_\beta^q}{\|\alpha\|}. \tag{30}$$

The isotropic case ($\Delta_i = \Delta$) reduces to

$$\nu_e^{iso} = \tilde{c} \Delta^2 A_\gamma^{(1/2)-2q} B_\gamma^q; \quad \gamma = \alpha^T \alpha; \quad \tilde{c} = 2^{2q-1} c. \tag{31}$$

This shows that the model is essentially built of the first two principal invariants of the positive semidefinite matrix $\alpha^T \alpha$.

To prove that the isotropic case is rotation invariant, we introduce a rotation matrix ρ and define the rotation of coordinates by $\tilde{x} = \rho x$ and $\tilde{u} = \rho u$. As $\rho^{-1} = \rho^T$, the velocity derivative matrix in the new coordinates reads $\tilde{\alpha} = \rho \alpha \rho^T$. Consequently $\tilde{\alpha}^T \tilde{\alpha}$ equals $\rho \alpha^T \alpha \rho^T$, which implies that the invariants of $\alpha^T \alpha$ and $\tilde{\alpha}^T \tilde{\alpha}$ are the same. This rotation invariance implies that the isotropic ν_e equals zero for all rotations of the flow types in $\{Q_n(B_\beta)\}$.

Although not rotation invariant, the anisotropic ν_e does vanish for all rotations of flow types in $\{Q_n(B_\beta)\}$. To prove

this, we consider a velocity field u which, after a rotation of coordinates, attains the form in Eqs. (14) or (15). Thus for some rotation matrix ρ , we have $\tilde{x} = \rho x$, $\tilde{u} = \rho u$, and $\tilde{\alpha} = \rho \alpha \rho^T$, such that $\tilde{\alpha}$ has the form (14) or (15). Defining a diagonal matrix ξ with Δ_1^2, Δ_2^2 , and Δ_3^2 on the diagonal, the anisotropic β can be rewritten as

$$\beta = \alpha^T \xi \alpha = \tilde{\alpha}^T \tilde{\xi} \tilde{\alpha}, \quad \tilde{\xi} = \rho \xi \rho^T, \tag{32}$$

where $\tilde{\xi}_{ij}$ is in general a full matrix. If $\tilde{\alpha}$ is of the type (14), an explicit calculation of $\beta = \tilde{\alpha}^T \tilde{\xi} \tilde{\alpha}$ gives

$$\begin{pmatrix} 0 & 0 & 0 \\ 0 & \tilde{\alpha}_{12}^2 \tilde{\xi}_{11} & \tilde{\alpha}_{12} \tilde{\alpha}_{13} \tilde{\xi}_{11} \\ 0 & \tilde{\alpha}_{12} \tilde{\alpha}_{13} \tilde{\xi}_{11} & \tilde{\alpha}_{13}^2 \tilde{\xi}_{11} \end{pmatrix}, \tag{33}$$

while for $\tilde{\alpha}$ of the type (15) we find that β equals

$$\begin{pmatrix} 0 & 0 & 0 \\ 0 & 0 & 0 \\ 0 & 0 & \tilde{\alpha}_{13}^2 \tilde{\xi}_{11} + \tilde{\alpha}_{13} \tilde{\alpha}_{23} (\tilde{\xi}_{21} + \tilde{\xi}_{12}) + \tilde{\alpha}_{23}^2 \tilde{\xi}_{22} \end{pmatrix}. \tag{34}$$

It can simply be verified that for both cases $B_\beta = 0$ and thus the anisotropic ν_e equals zero as well.

The parameter q in definition (28) controls the activity of the model near walls and transitional regions, where it is less active for higher q . To quantify this, suppose that the flow is of the type (14) or (15) plus a perturbation of small amplitude a . Then it is easy to prove that $\nu_e \sim a^{2q}$. The eddy viscosity is first order in the perturbation of a locally laminar shear flow in case $q = \frac{1}{2}$. In addition, the eddy viscosity is exactly zero at a no-slip wall. At a wall the streamwise and spanwise derivatives, say $\partial_1 u_i$ and $\partial_3 u_i$, are zero. As the incompressibility constraint implies zero $\partial_2 u_2$, the nonzero derivatives can only be $\partial_2 u_1$ or $\partial_2 u_3$. The velocity derivative matrix at the wall is equivalent to the type (14), thus $\nu_e = 0$.

Model (5) corresponds to $q = \frac{1}{2}$:

$$\nu_e = c \frac{\sqrt{B_\beta}}{\|\alpha\|} \leq \frac{c \|\alpha\|}{\sqrt{3}} \max\{\Delta_1^2, \Delta_2^2, \Delta_3^2\}. \tag{35}$$

The upper bound shows that there is no true singularity in the model; ν_e should be taken zero for $\|\alpha\| = 0$. A simple estimate for the model constant c is obtained, if we assume that ν_e approximately equals its upper bound in the case of homogeneous isotropic turbulence. In addition, substituting $\Delta_i = \Delta$ and $\|\alpha\| \approx \|S\|$, the Smagorinsky model is recovered for $c \approx 2.5 C_S^2$. As $C_S = 0.17$ is the theoretical value¹³ for homogeneous isotropic turbulence, we find $c = 0.07$. To obtain robust simulations in complex cases the practical value of C_S is sometimes higher than the theoretical one. For example, $C_S = 0.2$ has frequently been used in literature, which corresponds to $c = 0.1$ for the present model. Lower values of C_S have also been used, $C_S = 0.1$, for example, which corresponds to $c = 0.025$. Note that a larger model constant c or C_S^2 is equivalent to a larger Δ/h ratio.

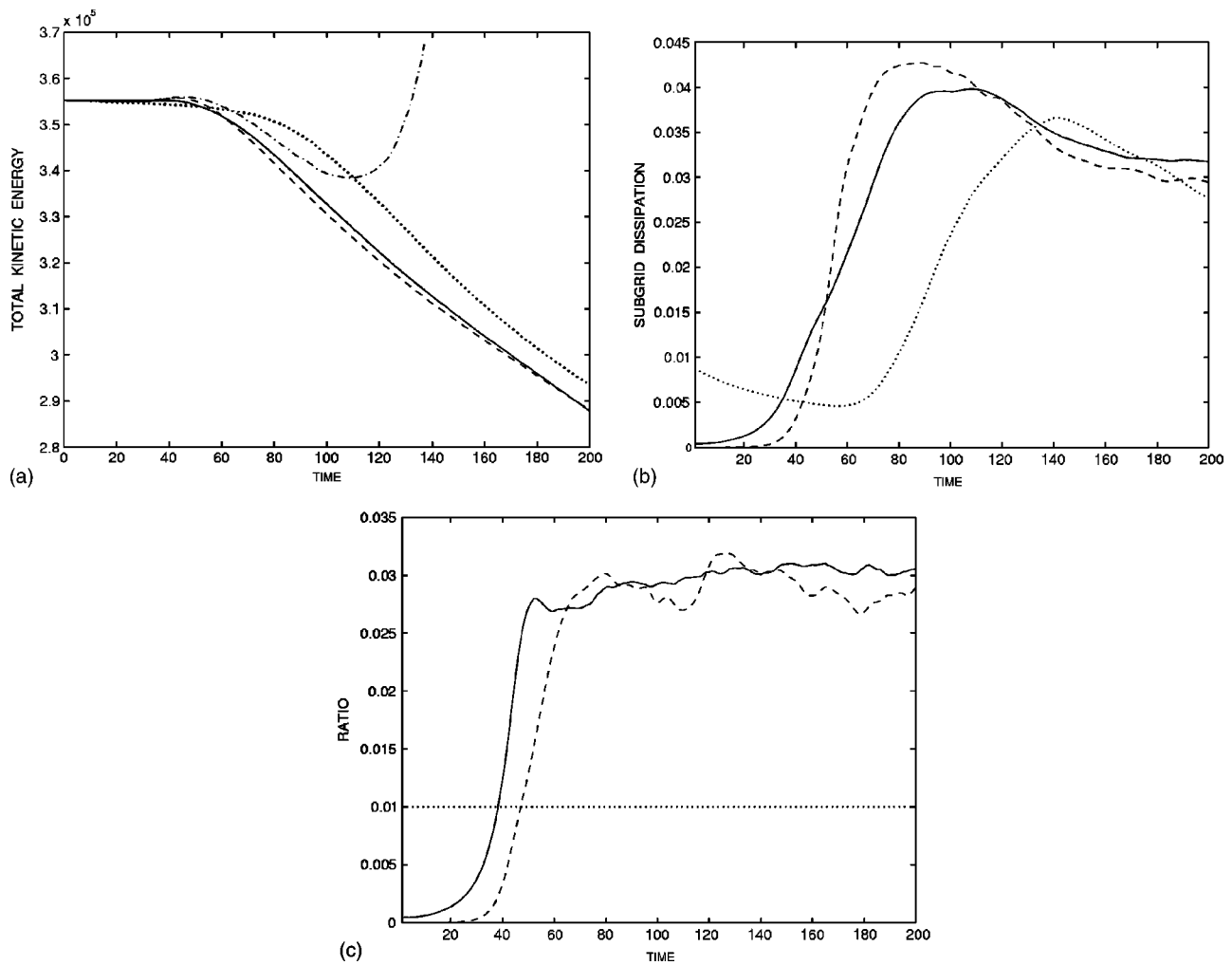


FIG. 1. Mixing layer results that demonstrate that unlike the Smagorinsky model, the dissipation of the present model is small in transitional flow; (a) total kinetic energy $\int \bar{u}_i \bar{u}_i dx$ normalized by $\frac{1}{4}(U_1 - U_2)^2 \delta_0^3$, (b) subgrid dissipation $\int \langle \nu_e |S|^2 \rangle dx_2$ normalized by $\frac{1}{8}(U_1 - U_2)^3$, and (c) ratio $\langle \nu_e \rangle / \langle \Delta^2 |S| \rangle$ in the center plane. Present model (solid), dynamic Smagorinsky (dashed), standard Smagorinsky (dotted), and 0-model (dash-dotted).

III. APPLICATIONS

The performance of the model emerging from the previous theoretical results is now illustrated for two cases: a transitional and turbulent mixing layer at high Reynolds number and a turbulent channel flow at $Re_\tau = 360$. It will be demonstrated that model (5) can successfully be applied in actual LES and is able to handle the complications caused by high Reynolds number, transition, and walls.

In this entire section the parameters in the model equal $q = \frac{1}{2}$ and $c = 0.07$. Second-order accurate incompressible and compressible flow solvers are used in order to mimic the low order of accuracy that is usually achieved in industrial codes. The present model will be compared with the Smagorinsky model³ and the dynamic eddy-viscosity model proposed by Germano *et al.*⁴

The first application is a LES of an experiment by Urban and Mungal:¹⁴ a weakly compressible mixing layer at high Reynolds number. The simulations are temporal, the convective Mach number equals 0.25, and the initial mean velocity profile $u_1 = \tanh(x_2)$ is perturbed with uniform noise of a small amplitude (0.01), restricted to the center region of the shear layer. The velocity difference $U_1 - U_2$ equals 2, while

δ_0 , which denotes half the initial vorticity thickness, equals 1. The domain contains 90^3 uniform cubic grid cells of size $\Delta = h = 1$. The Reynolds number $Re_\Delta = 10^5$ is high, as in the experiment. The small value of the Kolmogorov length scale, about 0.001Δ , indicates that direct numerical simulation (DNS) of this flow remains impossible in the near future.

The numerical method is the second-order finite volume method *A* described in Ref. 15, where it was found to be as accurate as a fourth-order method in case $\Delta = h$. The boundary conditions and implementation of the dynamic model are the same as in Ref. 16. For very small values of the new eddy viscosity, machine precision errors inherent in floating point operations may contaminate the calculation of B_β in practice. For this reason the simulations in this section used $\nu_e = 0$ if $B_\beta < 10^{-8}$. This statement also numerically reproduces the correct analytical limit for $\|\alpha\| \rightarrow 0$.

Figures 1–3 show that the present model performs better than the standard Smagorinsky model and is as good as the dynamic Smagorinsky model. The dynamic model is known to produce relatively accurate results in mixing layers at low Reynolds numbers, where comparison with DNS data is feasible.¹⁶ The computational effort needed for the entire

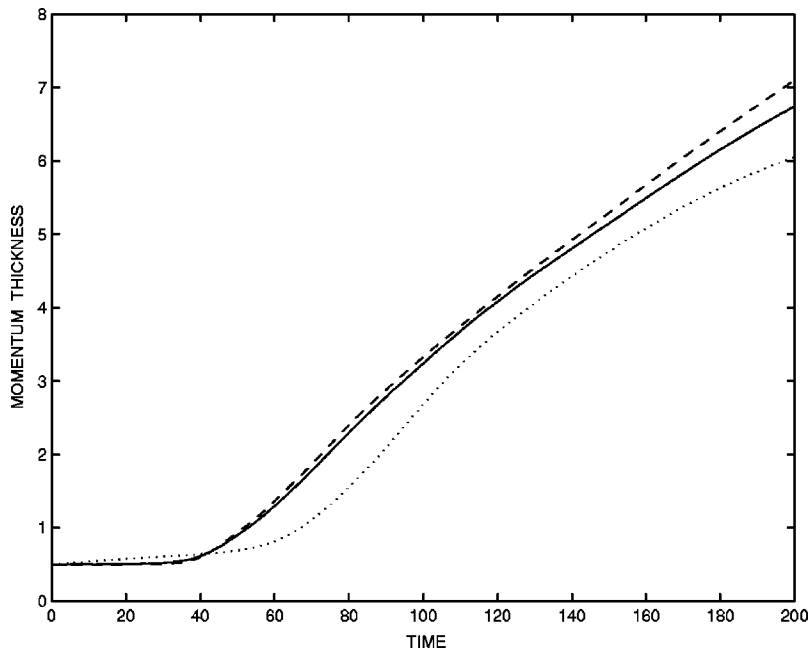


FIG. 2. Mixing layer. (a) Momentum thickness normalized by δ_0 . Present model (solid), dynamic Smagorinsky (dashed), and standard Smagorinsky (dotted).

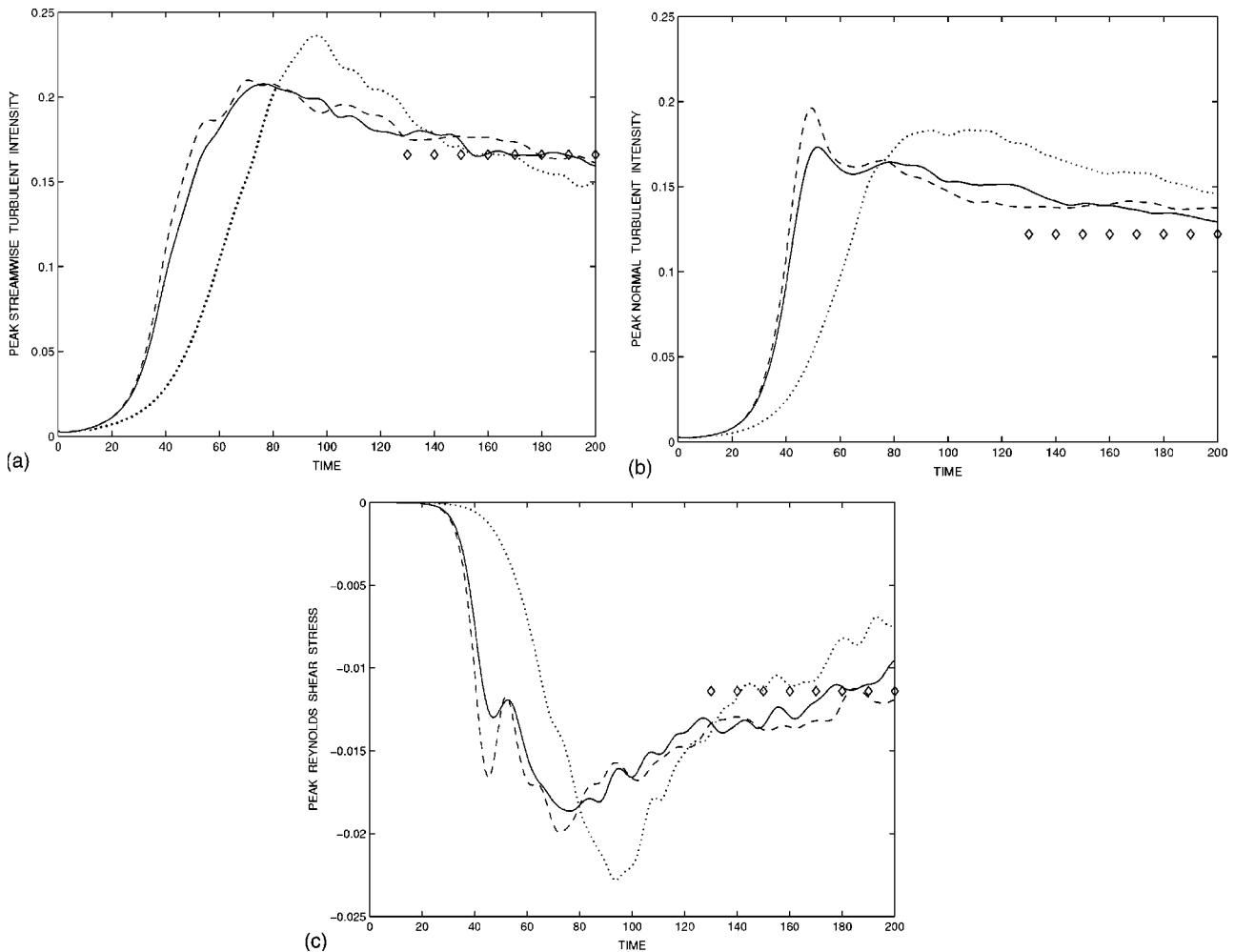


FIG. 3. Mixing layer. (a) Streamwise and (b) normal turbulent intensity in the center plane (normalized by $U_1 - U_2$); (c) Reynolds shear stress in the center plane (normalized by $(U_1 - U_2)^2$). Present model (solid), dynamic Smagorinsky (dashed), standard Smagorinsky (dotted), and experiment by Urban and Mungal (Ref. 14) (diamonds).

simulation with the present model in the current compressible code was only 50% of the cost of the dynamic simulation. Like the Smagorinsky model, the present model is relatively cheap.

For the Smagorinsky model the relatively low value $C_S = 0.1$ is used to give this model a fair chance for turbulent shear flow. Note that the Smagorinsky eddy viscosity for $C_S = 0.1$ is approximately three times lower in transition than for $C_S = 0.17$. Despite this low value, the Smagorinsky model is much too dissipative in transition due to the presence of mean shear [Fig. 1(a)]. As a consequence the physical instability mechanisms are suppressed and the turbulence is delayed. Considerably more dissipation and delay were observed for $C_S = 0.17$, which in fact would be the correct value of C_S in the turbulent stage.

Unlike the Smagorinsky model, the present model is adequate in transition, where its dissipation is relatively small [Fig. 1(b)]. This is achieved without adopting a model constant that is lower than its theoretical isotropic estimate. The evolution of the total subgrid dissipation also shows that the total subgrid dissipation increases more slowly than for the dynamic model. This indicates that the model is less flexible than the dynamic model, but a larger value of q in Eq. (30) will enlarge its flexibility and produce a sharper curve of the subgrid dissipation.

The mean level of the new eddy viscosity in the turbulent regime is close to the mean level that a Smagorinsky eddy viscosity with $C_S = 0.17$ would produce. This is demonstrated in Fig. 1(c), which contains the evolution of $\langle \nu_e \rangle / \langle \Delta^2 |S| \rangle$ in the center plane. Figure 2 shows the evolution of the momentum thickness. It hardly grows during transition (until $t = 30$), while a strong, approximately linear growth is observed in the fully turbulent regime.

For complex turbulent flows or high Reynolds numbers, LES without a subgrid model (the 0-model) is often not sufficiently robust, unless special numerical techniques are employed that introduce artificial numerical dissipation. For the present mixing layer case the total kinetic energy of an LES with the 0-model blew up after some time and the simulation could not be completed [Fig. 1(a)].

Figure 3 shows that the predictions by the present model reasonably agree with the experimental results. The center line values of the streamwise and normal turbulent intensity and Reynolds shear stress have been plotted, because these values can simply be compared with the experimental results found in Ref. 14. The unresolved parts of the Reynolds stresses have not been included, which would marginally improve the predictions. The standard estimate of the unresolved part of the Reynolds shear stress is given by $\langle -\nu_e S_{12} \rangle$,¹⁷ which was never more than 2%. In contrast to the Reynolds stresses, the turbulent dissipation is almost entirely in the subgrid scales; the resolved dissipation equals less than 0.1% of the subgrid dissipation in the turbulent regime.

In addition, simulations of the mixing layer flow have been performed using $c = 0.1$, instead of 0.07, and/or another initial perturbation. The conclusions regarding the performance of the models remain the same.

Figures 4 and 5 contain an example of implementation for turbulent plane channel flow with $Re_\tau = 360$. These results

are obtained with an incompressible code that uses a second-order accurate energy-conserving discretization of the convective terms. The viscous terms are treated with the discrete seven-point Laplacian, while the discretization of the subgrid terms is according to Ref. 16. The collocated nonuniform grid contains $47 \times 63 \times 47$ cells in the domain $6H \times 2H \times 2H$, using $\Delta_i = h_i$. The fifth grid point in the normal direction is at $y^+ = 11$. The temporal discretization employs Adams–Bashforth one for the convective and forward Euler for the viscous and subgrid terms. The initial condition consists of the mean flow profile $(y/H)^{1/7}$ plus a sinusoidal perturbation. Statistical averaging is performed from $10H/u_\tau$ until $30H/u_\tau$. The flow is driven by a constant pressure gradient.

Figures 4 and 5 show that the present model is also able to produce adequate results for wall-bounded shear flow. Taking into account that the numerical method is only second order, there is reasonable agreement with the DNS data. The statistics from the DNS at $Re_\tau = 360$ (Hu and Sandham¹⁸) have been downloaded from www.afm.ses.soton.ac.uk/~zhi/channeldata. The documentation¹⁸ shows that mean flow and turbulent intensities collapse with those from the case $Re_\tau = 395$ published by Moser *et al.*¹⁹ The Reynolds number of the channel flow is sufficiently low to allow a LES without a subgrid model. Figures 4 and 5 include this simulation.

Like the dynamic model but unlike the standard Smagorinsky model, the present model shows an appropriate near-wall behavior. The mean flow profiles for the present and dynamic models are close to the DNS data, while the mean flow for the Smagorinsky model is much too low [Fig. 4(a)]. Figure 4(b) shows the three different eddy viscosities. Both the present eddy viscosity and dynamic eddy viscosity are reduced in the near-wall region, in contrast to the Smagorinsky eddy viscosity. The value of the present eddy viscosity is zero at the wall, in agreement with the analytical prediction from Sec. II. Thus the near-wall behavior of the present model is appropriate, although there are differences with the dynamic model.

Figure 4(c) estimates the turbulent dissipation for the large-eddy simulations. The turbulent dissipation can be written as a resolved plus an unresolved part. The resolved part is defined as $\langle \nu |S'|^2 \rangle$ where S'_{ij} denotes $S_{ij} - \langle S_{ij} \rangle$. The unresolved part is the average of the dissipation term in the k_τ equation. Assuming that the production and dissipation of subgrid scales are in equilibrium, we can estimate the unresolved turbulent dissipation by $-\langle \tau_{ij} S_{ij} \rangle$. This leads to $\langle \nu_e |S|^2 \rangle$, known as the subgrid dissipation, that is, the dissipation from resolved towards subgrid scales. According to Fig. 4(c), the turbulent dissipations for the present and dynamic models are not far from the DNS data and better than for the 0-model. In the case of the present model and dynamic model, the subgrid dissipation is about 40% and 30% of the total turbulent dissipation, respectively.

Table II summarizes the skin-friction coefficients, obtained from the mean velocity profiles. The present model predicts both coefficients within 2% error of the DNS values. The dynamic model is also good, much better than the 0-model, which shows errors of about 10%. The Smagorinsky model is completely out of range. The nonzero contribu-

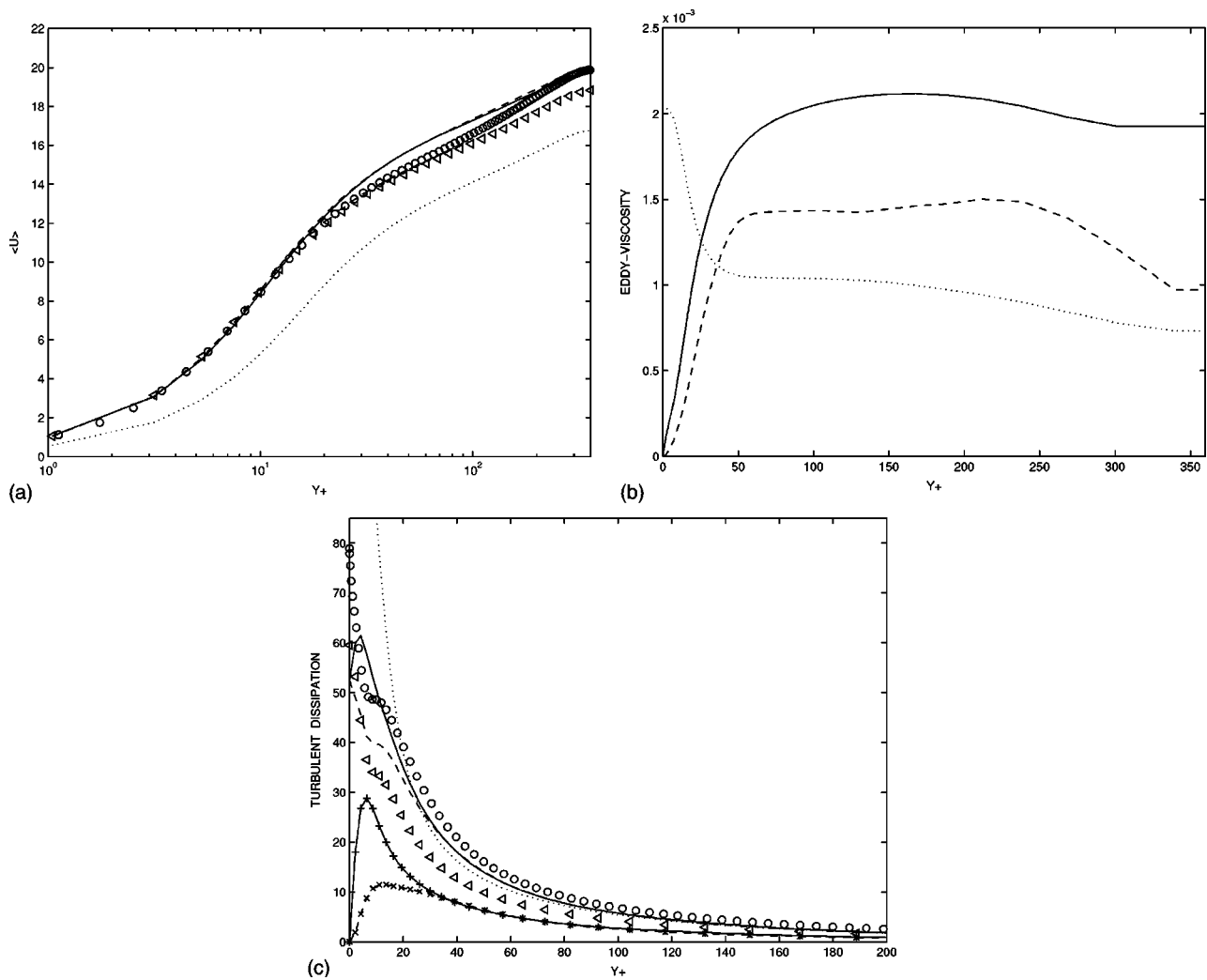


FIG. 4. Channel flow. (a) Mean streamwise velocity (normalized by u_τ), (b) subgrid eddy viscosity $\langle \nu_e \rangle$ (normalized by $u_\tau H$), and (c) turbulent dissipation and subgrid dissipation (normalized by u_τ^3/H). DNS (Ref. 18) (circles), present model (solid), dynamic Smagorinsky (dashed), standard Smagorinsky (dotted), and 0-model (triangles). The subgrid dissipation $\langle \nu_e |S|^2 \rangle$ is shown for the present model (pluses) and for the dynamic model (crosses).

tion of the Smagorinsky model to the wall shear stress has of course been included.

The left-hand side of Fig. 5 compares resolved turbulent intensities and shear stress with the *unfiltered* DNS data. This approach is usually followed in literature. A better agreement would be obtained if the resolved quantities were compared with *filtered* DNS data. However, there is a third approach, namely, to compare unfiltered DNS or experimental data with the sum of the resolved and unresolved part of the Reynolds stress tensor.

The unresolved part of the Reynolds stress tensor can be approximated by $\langle \tau_{ij} \rangle$ (see, e.g., Ref. 16, pp. 382–383, and Ref. 17), which becomes $\langle -2\nu_e S_{ij} + \frac{2}{3}k_\tau \delta_{ij} \rangle$ for eddy-viscosity models. A problem is that the unknown trace of the turbulent stress tensor has been lumped into the pressure. However, the realizability inequality (27) offers the model $k_\tau = c_1 \nu_e \|S\|$ with $c_1 \geq 1$. Taking $c_1 = 2\sqrt{2}$, we have $k_\tau = 2\nu_e |S|$, which according to Ref. 8 is a good approximation in case of the Smagorinsky model in a turbulent mixing layer. It is remarked that the estimate of k_τ can also be used to derive \bar{p} from the modified pressure $\bar{p} + \frac{2}{3}k$. Another option to correct the resolved Rey-

nolds stresses is to add a fraction of $\langle \beta_{ij} \rangle$ (compare Ref. 16), which in case of the present model would not involve extra calculations.

The right-hand side of Fig. 5 contains the “corrected” turbulent intensities and corrected Reynolds shear stress, obtained after adding up the resolved and unresolved parts of the Reynolds stresses using $k_\tau = 2\nu_e |S|$. In fact all profiles benefit from these corrections. In particular, the peak values of the normal and spanwise profiles significantly increase, while the Reynolds shear stress for both the present and dynamic models also considerably improves. Figure 5(d) clearly illustrates that the Smagorinsky model considerably contributes to the wall-shear stress in contrast to the dynamic and the present models. The 0-model somewhat overpredicts the turbulent shear stress.

Figure 5 thus demonstrates that the present model predictions of the turbulent intensities and Reynolds shear stress are satisfactory and in fact quite similar to the dynamic case. It is remarkable that the Smagorinsky model without wall damping also gives rise to acceptable second-order statistics. The poor near-wall behavior of this model apparently affects

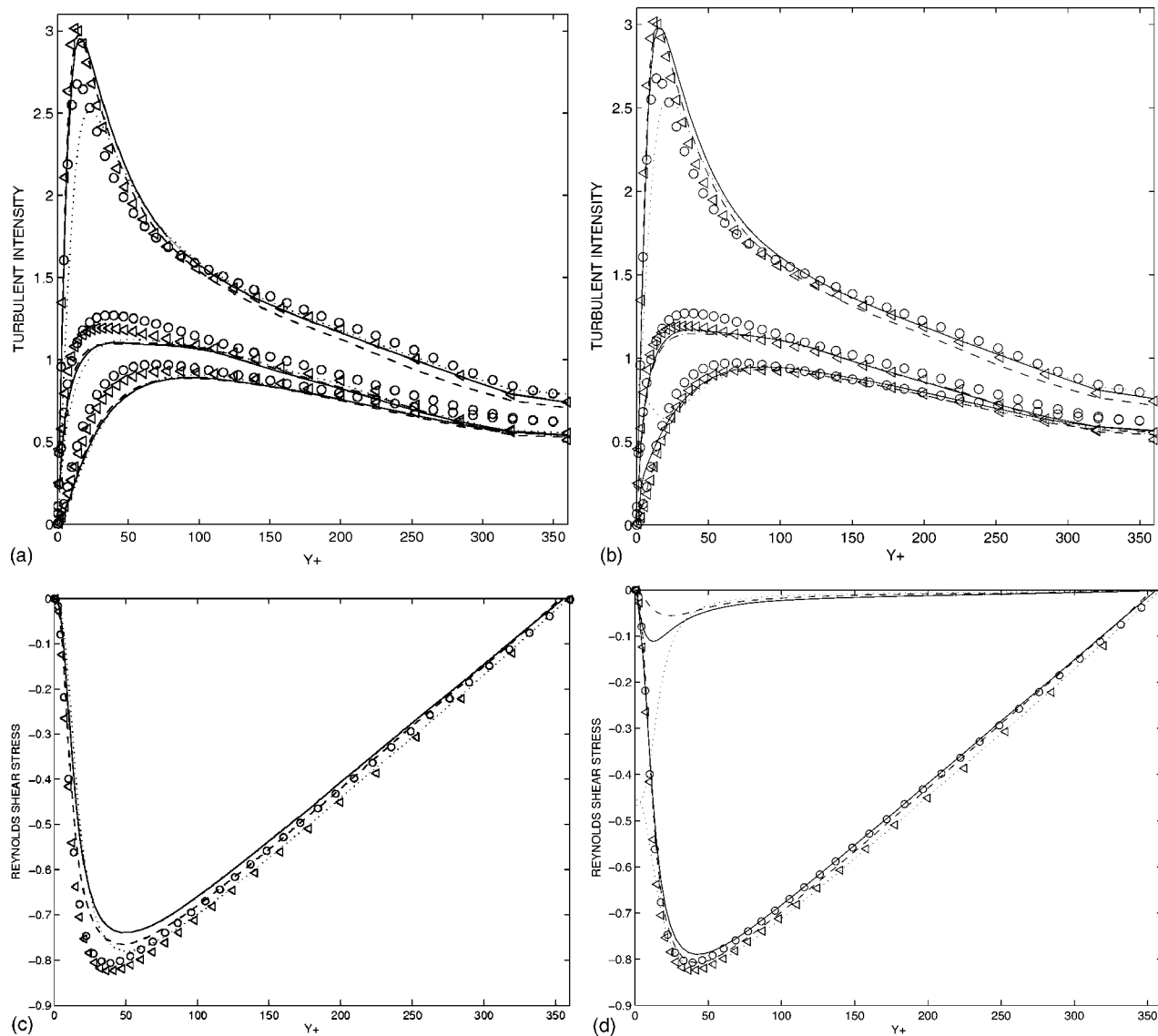


FIG. 5. Channel flow. Resolved (a) and corrected (b) turbulent intensities (normalized by u_τ). Streamwise intensity (highest set of curves), spanwise intensity (middle set), and normal intensity (lowest set). Resolved (c) and corrected (d) Reynolds shear stress (normalized by u_τ^2). DNS (Ref. 18) (circles), present model (solid), dynamic Smagorinsky (dashed), standard Smagorinsky (dotted), and 0-model (triangles). Top curves in (d) show the corrections $\langle -\nu_e S_{12} \rangle$.

the mean flow much more than the Reynolds stresses. Not only the Smagorinsky but the 0-model also produces acceptable second-order statistics. According to the left-hand side of Fig. 5, the 0-model seems the best. However, after inclu-

sion of the unresolved contributions, the second-order statistics of the present and dynamic models significantly improve and are not worse than those of the 0-model.

Summarizing Figs. 4 and 5 and Table II, we have found

TABLE II. Channel flow. Skin-friction coefficients c_f and C_f , based on center line and bulk velocity, respectively, and computed Reynolds number. The percentages denote the relative deviation from the DNS results. In all cases τ_w was calculated using $\frac{1}{2}(u_l+u_r)/d$, where u_l and u_r are mean velocities at the first grid point off the left/right wall and d the distance to the nearest wall. The bulk velocity in each case was calculated with the trapezoidal rule.

| | Computed Re_τ | c_f | C_f |
|-------------------|--------------------|-----------------|-----------------|
| DNS ^a | 364 | 0.005 06 | 0.006 67 |
| Present model | 361 | 0.005 14(+1.6%) | 0.006 57(-1.5%) |
| Dynamic model | 359 | 0.005 02(-0.8%) | 0.006 36(-4.6%) |
| Smagorinsky model | 365 | 0.007 11(+41%) | 0.009 51(+43%) |
| 0-model | 363 | 0.005 64(+11%) | 0.007 24(+8.5%) |

^aReference 18.

that the best all-round predictions for channel flow are given by the present and dynamic models. On the whole these models outperform the 0-model and are much better than the Smagorinsky model (without wall damping). It is stressed once more that LES with the 0-model is in general not robust, which was shown by the mixing layer case in this section. Nevertheless, for low Reynolds numbers and low order methods the 0-model is sometimes able to produce reasonable statistics, which is shown in Fig. 5. However, in a LES that uses the 0-model (without a tuned numerical upwind scheme), the amount of small scales in the resolved field is usually too large. In this way the molecular dissipation is able to take over the role of the subgrid dissipation.¹⁶ Due to the excessive amount of small scales, results obtained with the 0-model will be considerably more sensitive to the numerical discretization than results obtained with eddy-viscosity models.

The isotropic form of the present model, which corresponds to $\Delta_f = \Delta$ in Eq. (5), can also be applied to turbulent channel flow. For this purpose the standard expression $\Delta = (h_1 h_2 h_3)^{1/3}$ can be used. In that case the isotropic filter width in the near-wall region will be quite large in terms of h_2 . If this is undesirable, Δ can be taken equal to the minimum of $(h_1 h_2 h_3)^{1/3}$ and the distance to the nearest wall, which ensures that the support of the implicit isotropic top-hat filter remains inside the flow domain.

We have thus shown that the model produces satisfactory results for two different flow cases, using a single value of the model constant, which was equal to its theoretical estimate in isotropic turbulence. Apparently, the present model is much more able to adapt to different flow types than the Smagorinsky model.

In the previous two test cases the present model was found to perform as good as the dynamic model. In the particular case of plane channel flow better results might be achieved if the approximate deconvolution model (ADM)²⁰ is used. However, ADM is much more complicated than the model proposed in the present paper; it involves filter inversion by explicit filtering operations and a dynamic relaxation term. In addition, we recall that the accuracy of *a posteriori* LES is not only connected to the model but also to the numerics.¹⁵ The excellent ADM results were obtained with a spectral method, which is inapplicable in complex geometries. Model (5) is very easy to implement and this paper quantifies that it leads to satisfactory results, even for low order schemes. Thus, the present model seems well suited for engineering applications.

IV. CONCLUSIONS

A family of eddy-viscosity models has been proposed. They have the intrinsic ability to vanish for precisely the flow types with zero theoretical subgrid dissipation. For this purpose the models employ the second principal invariant of the gradient model. The specific model tested, Eq. (5), recognizes a perturbation of a laminar shear flow as a first-order effect. The models satisfy a fundamental realizability condition, which has been derived for the general eddy-viscosity hypothesis. The realizability condition suggests an alterna-

tive form of the eddy viscosity in the so-called one-equation models. In case of the Reynolds averaging operator, the inequality expresses an upper bound of the turbulent production in terms of the turbulent kinetic energy.

Although essentially not more complicated than the standard Smagorinsky model, the present model was found to be much more accurate in LES of inhomogeneous turbulence. The model was tested in two different flows, a turbulent channel flow and a transitional and turbulent mixing layer at high Reynolds number. In fact, it was observed to be approximately as accurate as the dynamic Smagorinsky model. A reasonable agreement with DNS data (channel flow) and experimental data (mixing layer) was observed, using second-order numerical methods. It is concluded that the model shows an appropriate transitional and near-wall behavior and remains robust in high Reynolds number applications.

The present model is a base model and it can obviously be used in conjunction with existing models in a so-called mixed framework. Further improvement of model (5) is possibly achieved if the dynamic procedure⁴ or the adjoint filtering technique⁹ is applied. The latter technique leads to the model $-F^a(2\nu_e FS_{ij})$, which includes backscatter. However, the main result of this paper is that a simple eddy-viscosity model exists which does not need such techniques to provide acceptable results for two inhomogeneous flows using a single value of the model constant. The eddy viscosity has the intrinsic ability to adapt to the local level of turbulent activity, while it does not need more than the local filter width and the first-order derivatives of the velocity field. Because of these properties, applications of the model in LES of more complex flows seem promising.

ACKNOWLEDGMENTS

The author is grateful to Dr. J. G. M. Kuerten for his comments on the manuscript and to the University of Twente for giving the author access to their facilities.

APPENDIX: FLOW ALGEBRA

The complete flow algebra $\{Q_n(B_\beta)\} = \{Q_n(D_\tau)\}$ is listed below:

$$\left\{ \left\{ \begin{pmatrix} 0 & 1 & 1 \\ 0 & 0 & 0 \\ 0 & 0 & 0 \end{pmatrix}, \begin{pmatrix} 0 & 1 & 0 \\ 0 & 0 & 0 \\ 0 & 1 & 0 \end{pmatrix}, \begin{pmatrix} 0 & 0 & 1 \\ 0 & 0 & 1 \\ 0 & 0 & 0 \end{pmatrix} \right\}, \right. \\ \left. \left\{ \begin{pmatrix} 0 & 0 & 0 \\ 1 & 0 & 1 \\ 0 & 0 & 0 \end{pmatrix}, \begin{pmatrix} 0 & 0 & 0 \\ 1 & 0 & 0 \\ 1 & 1 & 0 \end{pmatrix}, \begin{pmatrix} 0 & 0 & 0 \\ 0 & 0 & 0 \\ 1 & 1 & 0 \end{pmatrix} \right\}, \right. \\ \left\{ \begin{pmatrix} 0 & 1 & 0 \\ 0 & 0 & 0 \\ 0 & 0 & 0 \end{pmatrix}, \begin{pmatrix} 0 & 0 & 1 \\ 0 & 0 & 0 \\ 0 & 0 & 0 \end{pmatrix}, \begin{pmatrix} 0 & 0 & 0 \\ 1 & 0 & 0 \\ 0 & 0 & 0 \end{pmatrix} \right\}, \\ \left. \left\{ \begin{pmatrix} 0 & 0 & 0 \\ 0 & 0 & 1 \\ 0 & 0 & 0 \end{pmatrix}, \begin{pmatrix} 0 & 0 & 0 \\ 0 & 0 & 0 \\ 1 & 0 & 0 \end{pmatrix}, \begin{pmatrix} 0 & 0 & 0 \\ 0 & 0 & 0 \\ 0 & 1 & 0 \end{pmatrix} \right\}, \left\{ \begin{pmatrix} 0 & 0 & 0 \\ 0 & 0 & 0 \\ 0 & 0 & 0 \end{pmatrix} \right\} \right\}.$$

As B_β is only expressed in first-order derivatives, an algebraic computer program could evaluate for each of the 320 flow types whether B_β vanished or not. The binary matrices corresponding to the derivative matrices for which $B_\beta=0$ are exactly those listed above.

Next it is proven that the flow algebra of D_τ is not larger than these 13 matrices. According to definition (17), a binary matrix ζ is not in the flow algebra of D_τ if a filter and a velocity field u_i corresponding to ζ exist such that $D_\tau \neq 0$.

We first consider the velocity derivative matrices with precisely two nonzero elements, say $\{\partial_k u_i, \partial_l u_j\}$. If one of these elements is a diagonal element, the definition of D_τ and the first term in the Taylor expansion⁵⁻⁷

$$\tau_{ij} = \frac{\Delta_k^2}{12} \partial_k u_i \partial_k u_j + O(\Delta^4) \quad (\text{A1})$$

imply that in general $D_\tau \neq 0$. If both nonzero elements are on the diagonal, the incompressibility constraint may cause zero D_τ , but only if $\Delta_k = \Delta_l$. Anisotropic filters with $\Delta_k \neq \Delta_l$ produce $D_\tau \neq 0$. We conclude that matrices with at least one nonzero diagonal element are not in $\{Q_n(D_\tau)\}$.

In order to verify the nonzero pairs that do not contain a diagonal element, a spherical top-hat filter with radius R and filter volume V is employed. The Taylor expansion of the filtered velocity becomes

$$\bar{u}_i = u_i + \frac{R^2}{10} \partial_m^2 u_i + \frac{R^4}{280} \partial_k^2 \partial_l^2 u_i + O(R^6), \quad (\text{A2})$$

because the expressions

$$\frac{1}{2!} \frac{3}{4\pi R^3} \int_V x_1^2 dV = \frac{R^2}{10}, \quad (\text{A3})$$

$$\frac{1}{4!} \frac{3}{4\pi R^3} \int_V x_1^4 dV = \frac{R^4}{280}, \quad (\text{A4})$$

$$\frac{1}{4!} \binom{4}{2} \frac{3}{4\pi R^3} \int_V x_1^2 x_2^2 dV = \frac{R^4}{140} \quad (\text{A5})$$

are the coefficients in front of $\partial_l^2 u_i$, $\partial_l^4 u_i$, and $\partial_l^2 \partial_m^2 u_i$, respectively. Substitution of Eq. (A2) into the turbulent stress tensor gives

$$\begin{aligned} \tau_{ij} = & \frac{R^2}{5} \partial_m u_i \partial_m u_j - \frac{R^4}{350} \partial_k^2 u_i \partial_l^2 u_j + \frac{R^4}{70} (\partial_l \partial_k^2 u_i \partial_l u_j \\ & + \partial_l u_i \partial_l \partial_k^2 u_j + \partial_k \partial_l u_i \partial_k \partial_l u_j) + O(R^6). \end{aligned} \quad (\text{A6})$$

After excluding the diagonal elements, there remain 15 possible nonzero pairs of velocity derivatives, which are represented by the following five different cases:

$$\begin{aligned} & \{\partial_1 u_2, \partial_1 u_3\}, \{\partial_1 u_2, \partial_3 u_2\}, \{\partial_1 u_2, \partial_2 u_3\}, \\ & \{\partial_1 u_3, \partial_2 u_1\}, \{\partial_1 u_2, \partial_2 u_1\}. \end{aligned} \quad (\text{A7})$$

The other ten pairs are covered by the application of cyclic interchange of indices ($1 \rightarrow 2 \rightarrow 3 \rightarrow 1$) to the five cases above. In Sec. II we proved that the first two cases in expression (A7) belong to the flow algebra of D_τ . However, the third case is not in the flow algebra, because a corresponding

velocity field and a filter exist such that $D_\tau \neq 0$. For $u_2 = x_1^2$ and $u_3 = x_2^2$, Eqs. (A2) and (A6) imply

$$D_\tau = \frac{R^4}{350} (\partial_2^2 u_3 \partial_1^2 u_2) \partial_2 \bar{u}_3 = \frac{4x_2 R^4}{350} \neq 0. \quad (\text{A8})$$

In a similar way it can be proven that the last two cases in expression (A6) do not belong to $\{Q_n(D_\tau)\}$. [It is easily verified that B_β also equals zero for the first two cases in Eq. (A2) and nonzero for the last three cases.]

Suppose a given matrix ζ with precisely n nonzeros is in the flow algebra of D_τ . As a consequence, the flow algebra also contains each matrix derived from ζ by replacing nonzero components of ζ with zero. This argument and the results for matrices with two nonzero elements do not allow that $n \geq 3$. This completes the proof that $\{Q_n(D_\tau)\}$ is not larger than the set of 13 matrices.

Of course one could restrict the local filter space Γ and only allow *separable* filters, which can be written as a product of three one-dimensional filters. If only separable filters are allowed, $\{Q^n(D_\tau)\}$ is much larger. In that case it is equal to $\{Q^n(D_\beta)\}$, the flow algebra of the dissipation of the gradient model D_β . This means that for separable filters the theoretical subgrid dissipation also vanishes for the matrices in Eq. (22). However, the most natural three-dimensional filter with a finite support is a uniform average over a sphere (the nonseparable spherical top-hat filter). The restriction of Γ to separable filters is apparently not the most logical choice.

¹C. Meneveau and J. Katz, "Scale-invariance and turbulence models for large-eddy simulation," *Annu. Rev. Fluid Mech.* **32**, 1 (2000).

²S. B. Pope, *Turbulent Flows* (Cambridge University Press, Cambridge, 2000).

³J. Smagorinsky, "General circulation experiments with the primitive equations," *Mon. Weather Rev.* **91**, 99 (1963).

⁴M. Germano, U. Piomelli, P. Moin, and W. H. Cabot, "A dynamic subgrid-scale eddy-viscosity model," *Phys. Fluids A* **3**, 1760 (1991).

⁵A. Leonard, "Energy cascade in large-eddy simulations of turbulent fluid flows," *Adv. Geophys.* **18**, 237 (1974).

⁶R. A. Clark, J. H. Ferziger, and W. C. Reynolds, "Evaluation of subgrid-scale models using an accurately simulated turbulent flow," *J. Fluid Mech.* **91**, 1 (1979).

⁷B. Vreman, B. Geurts, and H. Kuerten, "Large-eddy simulation of the temporal mixing layer using the Clark model," *Theor. Comput. Fluid Dyn.* **8**, 309 (1996).

⁸B. Vreman, B. Geurts, and H. Kuerten, "Realizability conditions for the turbulent stress tensor in large eddy simulation," *J. Fluid Mech.* **278**, 351 (1994).

⁹A. W. Vreman, "The adjoint filter operator in large-eddy simulation of turbulent flow," *Phys. Fluids* **16**, 2012 (2004).

¹⁰C. D. Pruett and N. A. Adams, "A priori analyses of three subgrid-scale models for one-parameter families of filters," *Phys. Fluids* **12**, 1133 (2000).

¹¹A. W. Vreman, B. J. Geurts, N. G. Deen, and J. A. M. Kuipers, "Large-eddy simulation of a particle-laden turbulent channel flow," in *Direct and Large-Eddy Simulation V*, edited by R. Friedrich, B. J. Geurts, and O. Metais (Kluwer, Dordrecht, 2004), pp. 271–278.

¹²U. Schumann, "Subgrid scale model for finite difference simulations of turbulent flows in plane channels and annuli," *J. Comput. Phys.* **18**, 376 (1975).

¹³D. K. Lilly, "The representation of small-scale turbulence in numerical simulation experiments," in *Proceedings of IBM Scientific Computing Symposium on Environmental Sciences*, edited by H. H. Goldstine (Yorktown Heights, New York, 1967), pp. 195–210.

¹⁴W. D. Urban and M. G. Mungal, "Planar velocity measurements in compressible mixing layers," *J. Fluid Mech.* **431**, 189 (2001).

¹⁵B. Vreman, B. Geurts, and H. Kuerten, "Comparison of numerical

- schemes in large-eddy simulation of the temporal mixing layer," *Int. J. Numer. Methods Fluids* **22**, 297 (1996).
- ¹⁶B. Vreman, B. Geurts, and H. Kuerten, "Large-eddy simulation of the turbulent mixing layer," *J. Fluid Mech.* **339**, 357 (1997).
- ¹⁷J. W. Deardorff, "A numerical study of three-dimensional turbulent channel flow at large Reynolds numbers," *J. Fluid Mech.* **41**, 453 (1970).
- ¹⁸Z. W. Hu and N. D. Sandham, "DNS databases for turbulent Couette and Poiseuille flow," University of Southampton, Report No. AFM-01/04, 2001 (unpublished).
- ¹⁹R. D. Moser, J. Kim, and N. N. Mansour, "Direct numerical simulation of turbulent channel flow up to $Re_\tau=590$," *Phys. Fluids* **11**, 943 (1999).
- ²⁰S. Stolz, N. A. Adams, and L. Kleiser, "An approximate deconvolution model for large-eddy simulation with application to incompressible wall-bounded flows," *Phys. Fluids* **13**, 997 (2001).